

**Alaska crustal deformation: Finite element modeling constrained by geologic and VLBI data**

Paul Lundgren

*Jet Propulsion Laboratory, California Institute of Technology*

*4800 Oak Grove Drive, Pasadena, California 91109*

*Tel: (818) 354-1795 FAX: (818) 393-50.59*

Franc ois Saucier

*Institut Maurice-Lamontagne*

*850, route de la Mer, C.P. 1000*

*Mont Joli, Quebec, G5H 3Z4, Canada*

Randy Palmer

*Department of Geological Sciences, University of Oregon, Eugene, Oregon 91723*

Marc Langon

*Jet Propulsion Laboratory, California Institute of Technology*

*4800 Oak Grove Drive, Pasadena, California 91109*

Abstract. We compute **crustal** motions in Alaska by calculating the **finite** element solution for an elastic spherical shell problem. The method we use allows the **finite** element mesh to include faults and very long baseline **interferometry (VLBI)** baseline rates of change. Boundary conditions include Pacific-North America (**PA-NA**) plate motions. The solution is **con-**strained by the oblique orientation of the **Fairweather-Queen Charlotte** strike-slip faults relative to the PA-NA relative motion direction and the oblique orientation from normal convergence of the eastern Aleutian trench fault systems, as well as strike-slip motion along the **Denali** and **Totschunda** fault systems. We explore the effects that a range of fault slip constraints and weighting of VLBI rates of change has on the solution. **This** allows us to test the motion on faults, such as the **Denali** fault, where there **are** conflicting **reports** on its present day slip rate. We find a pattern of **displacements** which produce fault motions generally consistent with **geo-**logic observations. The motion of the continuum has the general pattern of radial movement of crust to the NE away from the Fairweather-Queen Charlotte fault systems in SE Alaska and Canada. This pattern of **crustal** motion is absorbed across the Mackenzie Mountains in NW Canada, with **strike-slip** motion constrained along the **Denali** and **Tintina** fault systems. In south central Alaska and the Alaska fore-arc oblique convergence at the eastern Aleutian trench and the strike-slip motion of the **Denali** fault system produce a counter-clock-wise pattern of motion which is partially absorbed along the Contact and related fault systems in southern Alaska and is partially extruded into the Bering **Sea** and into the forearc parallel the Aleutian trench **from** the Alaska Peninsula westwards, Rates of motion and fault slip **are** small in western and northern Alaska but the motions we compute are consistent with the senses of strike-slip motion inferred geologically along the **Katag, Kobuk** Trench and Thompson Creek faults, and the normal faulting observed in NW Alaska near Nome. The non-rigid behavior of our finite element solution **produces** patterns of motion that would not have been expected

from rigid block models: strike-slip faults can exist in a continuum that has motion mostly **perpendicular** to their strikes and faults can exhibit along-strike differences in magnitudes and directions.

## Introduction

Deformation across the Pacific - North America (PA-NA) convergent boundary is spread across a broad region extending hundreds of kilometers inland from the plate boundary. The plate boundary orientation varies **considerably**, from oblique convergence in southeastern and south central Alaska, to normal convergence off the **western** Alaska Peninsula, and back to highly oblique convergence in the **western** Aleutian arc [Perez and Jacob, 1980; Jarrard, 1986; DeMets *et al.*, 1990]. Considerable deformation is observed in the over riding North American plate, In eastern Alaska, PA-NA motion is accommodated by right lateral (RL) strike-slip motion on the Fairweather, Dalton Creek, Denali, and Tintina faults [Plafker *et al.*, 1978; Lisowski *et al.*, 1987; Plafker *et al.*, 1993]. The Yakutat Block occupies the transition region between the Queen Charlotte and Fairweather faults and the Aleutian megathrust to the west, although its separation from the Pacific plate along the Transition Zone fault remains unresolved [Plafker, 1987; Brims and Carlson, 1987]. While many data exist on fault orientations and slip rates in Alaska, much uncertainty remains regarding which faults are presently active and how fast they are slipping.

We present a study of the distribution of motion in the North America plate of Alaska and northwest Canada. We use a finite element method for obtaining a static, elastic, 2-d spherical shell solution of motion which incorporates plate motion boundary conditions as well as faults with differing degrees of constraint and geodetic rates in the form of VLBI baseline rates of change. The incorporation of a limited number of constrained faults and VLBI baselines allows us to obtain a general motion solution for the mesh which matches geologically inferred fault slip directions and rates and VLBI transverse components which are left unconstrained in the model.

## Method

To model the kinematics and deformation of crustal blocks we incorporate geologic and geodetic data in a finite element formalism [Saucier and Humphreys, 1993]. We solve the standard finite element equation

$$\mathbf{K}\mathbf{U} = \mathbf{f} \quad (1)$$

where  $\mathbf{K}$  is the global stiffness matrix,  $\mathbf{U}$  is the global displacement matrix which is to be solved for, and  $\mathbf{f}$  is the global force vector [i.e. Zienkiewicz and Taylor, 1989]. We solve for nodal displacements in an elastic, plane stress ( $\sigma_3 = 0$ ; see Turcotte and Schubert [1982]), 2-D spherical shell. We use 8 node biquadratic isoparametric elements (elements have a node on each corner and one on each of their four sides; isoparametric means that the shape functions which map the global spherical shell coordinates into the “local” coordinates are the same for the displacements which are solved for in the “local” coordinate system and mapped back into the global coordinate system). The displacement solution minimizes the strain energy in the plate and geodetic array and provides estimates for block deformation, motion, and fault slip rates everywhere in the finite element array. A Monte Carlo technique is used to interpret the sensitivity of the model due to uncertainties in the imposed fault and plate motion rate data.

Boundary conditions enter into the model as prescribed rates about a pole of rotation and/or constraints on nodal displacement degrees of freedom in either colatitude or longitude. Faults can be constrained in direction and rate by using “split” nodes [Melosh and Raefsky, 1981], or as free shear surfaces which can be constrained to slip parallel to a direction [Melosh and Williams, 1989] or can be left unconstrained. Both boundary node prescribed rates and split nodes enter into (1) in the force vector  $\mathbf{f}$  and reduce the number of equations which need to be solved in (1).

Geodetic baseline rates of change are considered as a network of elastic telescopic truss bars which constrain the rate between sites on the elastic plate and can be weighted relative to the geologic constraints. Weights enter the model through a weighting factor which is equivalent to increasing Young's modulus. Higher weighting has the effect of making the weighted elements more rigid. In the case of the baselines, they are formed as two-element truss bars. The two elements share 3 nodes at the center of the truss bar and the three nodes at each end of the truss bar are connected to the main mesh at the center node at each end. The three nodes at the center of each truss bar are split nodes which move at the prescribed baseline rate. The strain induced in the mesh by the change in baseline length is balanced by strain in the truss bar itself. By increasing the relative weight of the truss bar relative to the main mesh the truss bar transmits more of the prescribed baseline rate to the main mesh since the strain energy produced in the truss bar is now higher than in the mesh for the same amount of strain.

The most significant difference between this approach and the rigid plate model [i.e. DeMets *et al.*, 1990], is that it considers deformable blocks. Unlike the rigid plate inversion, local misfits between observed and predicted motions are "absorbed" locally, rather than being spread equally at all boundary locations of adjacent plates since the mesh is allowed to deform rather than remain rigid. The allowance of non-rigid deformation allows for more complex patterns of deformation. One such example is that strike-slip motion can occur along faults without the motion of the continuum on either side of the fault moving parallel the fault. This allows faults to have rates which vary along strike and may explain some aspects of fault variability observed in the field.

Geologic and geodetic constraints

Table 1. summarizes the main rates and slip directions for the faults considered in this study. The two studies which report geologic rates for the **Denali** and Totschunda fault systems [Plafker et al., 1977; Plafker et al., 1993] based their rates (with no uncertainties given) on the offsets of glacial debris features and the assumed time since the last Pleistocene glaciation in central Alaska, It should be noted that the **Denali** and Totschunda rates of 10-20 mm/yr which are often seen in the literature for the Plafker et al. [1977] study are based on their assumed age of 8000 y.b.p. for the last glaciation, The Plafker et al. [1993] neotectonic map uses some of these offsets plus some additional ones and uses a uniform age of 10,000 y.b.p. since the last glaciation. To be consistent we use the rates assigned in Plafker et al. [1993]. In this study we estimate uncertainties for these geologically measured rates for the **Denali** and Totschunda faults by assuming an uncertainty in the age of the last glaciation of 2000 years and an uncertainty in the offset of the glacial debris markers at 10 m (for features which are typically offset by 100-200 m). This gives an uncertainty of 3-5 mm/yr in these rates (depending on the offset amount). This number is probably comparable to the uncertainty used by Plafker et al. [1978] for the **Fairweather** fault were they used an age of 940\* 200 years to calculate that rate (with a 55 m offset). In the case of the geodetically determined rates for the **Fairweather** and Totschunda faults [Lisowski et al., 1987] their uncertainties are based on the uncertainties in their actual data and the modeled locking depth of the fault. For the **Denali** fault the geodetic data were found to be indistinguishable from no slip on the fault so no slip rate or uncertainty were determined [Savage and Lisowski, 1991].

The rate prescribed to the Queen Charlotte fault is based on the assumption that it essentially forms the PA-NA plate boundary where the North America plate margin does not show evidence of major well developed faults inland over which this motion might be distributed. The Aleutian trench is assumed to be converging at the PA-NA relative motion rate along the

western half of this fault in our mesh. The eastern part of the Aleutian trench from approximately Kodiak island to the Yakutat block is unconstrained.

The motion prescribed on the faults bounding the Yakutat Block are based on the assumption that this block is essentially a part of the Pacific plate [Lahr and Plafker, 1980], with the only measured displacements located across the FairWeather fault [Plafker et al., 1978; Lisowski et al., 1987]. No rate data are available for the Transition Zone (TZ) fault and different studies give different assessments as to whether or not it is currently active [Plafker, 1987; Bruns and Carlson, 1987]. In testing many different input models, we found that prescribed oblique convergence on this fault could be no more than 2 mm/yr without generating unacceptable slip directions at the northern end of the Chatham Strait fault (or up to 4 mm/yr if motion on the TZ fault was pure thrust). Therefore, we have found that the least amount of kinematic inconsistencies result if we fix the Yakutat block to the Pacific plate.

There are only three fault segments where there is geologic or geodetic control on the slip rate: Denali, Totschunda, and Fairweather faults. The Totschunda fault is modeled as RL strike-slip motion at a rate of  $10 \pm 3$  mm/yr, in agreement with both trilateration and Holocene slip rates. The FairWeather fault is modeled as RL slip at  $41 \pm 3$  mm/yr, which is at the lower end of the geodetically observed slip on this fault [Lisowski et al., 1987]. The Denali fault has rates from  $8-12 \pm 3$  mm/yr reported based on geologic observations, which differ significantly from the virtual lack of slip reported for geodetic measurements [Ma et al., 1990; Savage and Lisowski, 1991]. Examples we present will demonstrate the effects of constraining the Denali fault to slip at the Holocene rate [Plafker et al., 1993], or leaving the Denali rate unconstrained.

All other faults are either unconstrained in both sense of slip and rate or constrained as strike-slip faults (free to slip either right- or left-laterally), except for the Bruin Bay fault which



is constrained to move perpendicular to the fault strike [Plafker et al., 1993]. The **Tintina** fault which extends from eastern Alaska into British Columbia has been constrained as a strike slip fault along most of its length. In north-central British Columbia the fault is constrained to zero slip. This treatment of the **Tintina** fault allows displacements along its western extent where seismicity has been observed but Holocene rates are unknown [Brogan et al., 1975; Estabrook et al., 1988], and does not allow fault behavior where the fault has not been active in recent geologic time [Gabrielse, 1985]. The Contact fault system is chosen to absorb motion in extreme southern Alaska. This fault shows some evidence for Holocene activity in the Prince William Sound region [Bol and Roeske, 1993] although farther east the Border Ranges and St. Elias fault systems are also active but the scale of our study region necessitates incorporating one representative fault for this area into our mesh.

In Table 2 we show the VLBI rates used for the six baselines used in this study [J. Gipson, GSFC IERS '93 solution, pers. comm.] which has differences from previous VLBI solutions [i.e. Ma et al., 1990] due to differences in analysis which included more data from the **Yakataga** site and the ability to have breaks in station position while maintaining constant velocity to allow for co-seismic earthquake displacements such as the 1987 Gulf of Alaska earthquake sequence [J. Gipson, pers. comm.]. The VLBI rates we use are between the four sites which should be free from strain accumulation which affects sites located near the Aleutian trench [Ma et al., 1990]. We have explored the effects of heavily weighting the VLBI baselines, or with a weight of one with respect to crustal Alaska. We will demonstrate that heavy weighting produces a better fit to the VLBI baseline rates at the cost of producing geologically unacceptable motion on some faults.

## Models and Results

The finite element mesh used in this study is a spherical shell, In the figures the spherical shell is plotted as an oblique Mercator projection about the NUVEL- 1 PA-NA Euler pole [DeMets et al., 1990], such that the pole lies to the right of each figure and the right and left sides of the mesh are small circles about the PA-NA pole and lines parallel to them are lines of constant PA-NA relative motion, while the top and bottom sides arc lines of longitude with PA-NA relative motion varying along these directions. We use the following material properties: Youngs modulus,  $7 \times 10^{10}$  Pa; Poissons ratio, 0.25. To enforce rigidity in the oceanic Pacific plate a Youngs modulus of  $7 \times 10^{11}$  Pa was used.

A couple of comments about the above assumptions are warranted, The use of the NUVEL-1 model to determine the far-field relative PA-NA motion is justified by the data which provide the greatest constraint in the NUVEL- 1 model (Gulf of California spreading rates and transform azimuths, and global plate circuit closure) and the comparisons between the NUVEL- 1 rates (averaged over 3 Ma) and the space geodetic measurements which are in excellent agreement with each other [Smith et al., 1990; Dixon et al., 1991; Gordon and Stein, 1992]. The rigidity constraint on the Pacific plate in our models is employed to restrict deformation to the over riding continental North America plate. Deformation which is known to exist in the Gulf of Alaska in the Pacific plate [Saubert et al., 1993] is not considered in our model for lack of adequate constraint on the extent of this fault.

Figure 1 shows the mesh, faults, and VLBI baselines used in this study. The boundary conditions are: *sides 1* and *2* fixed; *side 3* free to move perpendicular to itself (1 degree of freedom), inboard of the Queen Charlotte fault there is no prescribed deformation, outboard on the edge of the Pacific plate there is a prescribed motion based on a node's latitude from the PA-NA pole; *side 4* unconstrained. Displacements for the Pacific plate are calculated from the NUVEL-1A model, which has slightly lower rotation rates than NUVEL-1 and is based on

recent changes in the geomagnetic time scale [DeMets et al., 1994]. Varying the boundary rates in this way produces a rigid body rotation of the Pacific plate with respect to the North America plate which does not produce internal deformation of the Pacific plate other than what is produced along its boundary with the North America plate.

We present four models. The first two, M1, and MIH represent the least number of fault rate constraints, in which the only constraint on the Denali fault is that it moves as a strike-slip fault. Model M1 has a VLBI weighting of one, while MIH has a VLBI weight of 1000. The third model presented, M2, has the Denali fault rates constrained in three locations based on the maps by Plafker et al. [1993] which are derived from Holocene offsets. The fourth model, M3, has the same constraints as M1, but with the additional constraint that the eastern Aleutian trench have pure reverse slip from near Kodiak Island to its triple junction with the Pamplona and Transition Zone faults.

Model M1 is controlled by the constraints imposed along the PA-NA boundary faults, along with some local forcing of motion due to the Totschunda fault. Figure 2a shows the imposed fault constraints and the material displacements at the center of each element. The shading of each element gives the standard deviation in rate resulting from uncertainties in the prescribed fault slip rates. We find that in southeastern Alaska, the Yukon, and NW British Columbia material is displaced radially away from the Queen Charlotte - Fairweather faults due to the oblique orientations of these faults with respect to the PA-NA motion direction. The relatively large (10-18 mm/yr) magnitudes calculated agree with the VLBI transverse rate observed for GILC-WHIT ( $10.2 \pm 2.9$  mm/yr observed;  $12.6 \pm 2.7$  calculated), and suggests that the general pattern and magnitudes of motion we compute in our model are consistent with observation. In the continental margin between the Aleutian trench and the Denali fault system the crust moves in a counterclockwise pattern. In the continental shelf of Alaska south of the

Contact fault **this** pattern is manifest by an E to NE motion with an increase in magnitude and northward component towards the **east** due to the oblique convergence (opposite sense from the FairWeather fault) at the Aleutian **trench**. Inboard of the Contact fault, between it and the **Denali-Totschunda** fault systems, the crust moves towards the northwest at 4-10 **mm/yr** in a counter-clock-wise rotation. **The** motion **this** model computed for Sourdough is about 7 **mm/yr** towards the W-NW, which is different from the 7-8 **mm/yr** towards the SW measured with **VLBI**, although the uncertainties for this vector are in excess of 1 **mm/yr** in both length and transverse components (see Table 2). The measured rate may be **corrupted** by a component of co-seismic displacement from the 1987 Gulf of Alaska earthquakes, although **Sauber et al.** [1993] did not find the modeled co-seismic offset for the Sourdough station (13.8  $\pm$  5.9 mm in north component 13.5  $\pm$  8.2 mm in east component) to be statistically significant at the **95%** confidence level from the **VLBI** rate (4.8  $\pm$  2.1 **mm/yr** in the direction S46W) averaged over the 1984-1990 time span which removed co-seismic offsets due to the 1987 earthquake. Material is displaced away **from** the **Contact-Fairweather** triple junction and does not substantially flow around **the** corner from NW British Columbia/SE Alaska into eastern Alaska.

In Figure 2b the resulting nodal fault slip rates for model M1 are plotted with the relative motion direction. The **Denali-Chatham Strait** fault system features very low rates of right-lateral motion along the **Chatham Strait** fault with up to 8 **mm/yr** displacements along the **central Denali** fault. The 6-8 **mm/yr** along the central **Denali** fault is intermediate between the insignificant (at 2  $\sigma$ ) right lateral strain rate reported by Savage and Lisowski [1991] and the 8.7-11.6  $\pm$  3 **mm/yr** geological] and derived Holocene rate [Plafker et al., 1977, Plafker et al., 1993]. Along the McKinley strand **of** the **Denali** fault just west of the **Broxson Gulch** fault we calculate 6 **mm/yr** of slip which also compares well with the 5-6  $\pm$  3 **mm/yr** of slip (uncertainty calculated in our study as described above for other **Holocene** age geologically measured

fault displacements) based on alluvial fan and drainage offsets over the last 10,000 years [Stout et al., 1973]. We see that the fast counter-clockwise displacements in the North America plate margin in south central **Alaska** are mostly absorbed at the Contact fault system. The Contact fault was left unconstrained in this model and has calculated displacement directions ranging from left-lateral (**LL**) slip near Kodiak Island to **northwest** directed convergence in western Prince William Sound to right-lateral oblique thrust in eastern Prince William sound and mostly normal convergence continuing towards its termination in SE Alaska. This sense of motion is in agreement with **field** observations of strike-slip motion in eastern Prince William sound and thrust motion on fault strands further east [Bol and Roeske, 1993].

Across other faults we **see** small displacements which have the sense of motion generally identified geologically. We **see** oblique left-lateral convergence in the Brooks Range, and oblique right-lateral convergence along the Eskimo Lakes fault. To the east the fault system extending through the Mackenzie Mountains absorbs the **crustal** displacements radiating away from the Queen Charlotte-Fairweather system, with convergence rates across the Mackenzie mountains as high as 10 **mm/yr**. Right-lateral strike-slip motion is observed along the **Kaltag**, **Kobuk** Trench, **Iditorod-Nixon-Fork** faults. Normal (near zero) motion is observed in the Seward Peninsula in agreement with observed normal faulting [Biswas et al., 1986; Estabrook et al., 1988; Page et al., 1991]. Left-lateral motion is found along the Thompson Creek fault in agreement with **neotectonic** observations [Plafker et al., 1993]. The Tintina fault features rates up to 7 **mm/yr** in the western Yukon although the rate varies considerably along its length.

Model MIH is the same as model MI but with a VLBI weight of 1000. This has the effect of drawing together sites such as **GILC-WHIT** to more closely match the VLBI baseline contraction of  $9.2 \pm 2.5$  **mm/yr**. The effect of this on the continuum rates is shown in Figure

3a where we see that the NE directed motion around WHIT in Figure 2a is now directed more northerly. The effects of this are perhaps more noticeable if we look at the fault slip rates in Figure 3b where we see that some faults such as the Kobuk Trench, **Broxson** Gulch, and parts of the **Denali** fault system have different senses of motion which are opposite the geologically inferred slip directions on these faults.

Model M2 (Figure 4) constrains portions of the **Denali** fault from just east of its junction with the Totschunda fault to west of the **Broxson** Gulch fault to Holocene slip rates of  $9.0 \pm 3.0$ ,  $8.7 \pm 3.0$ , and  $11.6 \pm 4.0$  mm/yr [Plafker et al., 1977; Plafker et al., 1993]. The effect of this is to produce normal faulting across the Thompson Creek fault and more of a thrust component across the eastern Kobuk Trench fault contrary to field observations (LL and RL strike-slip respectively). In the model these faults feature very low rates, and the amount of oblique slip on these faults is not well constrained by field observations [Gedney and Marshall, 1981; Plafker et al., 1993].

Model M3 constrains the eastern Aleutian trench to normal convergence. This constraint is supported by focal mechanisms of underthrusting earthquakes along the eastern Aleutian trench which have a horizontal slip direction which is directed more towards the NW than the relative convergence direction predicted by NUVEL-1 [DeMets et al., 1990]. In model M3 (Figure 5) we show the effect of this constraint on the motion of the south central Alaskan forearc. We find that this constraint produces a hinge-like effect with the result that the eastern part of the forearc rotates counterclockwise away from the trench reducing the relative slip rate at the eastern end of the Aleutian trench to under 15 mm/a and increasing slip on the Contact fault to over 30 mm/a, While the slip direction this model produces on the Contact [Bol and Roeske, 1993] and eastern Aleutian trench [DeMets et al., 1990] faults are basically consistent with geologic observations and global plate motion models respectively, the large slip in the

coast ranges of Alaska and the low slip on the eastern Aleutian trench do not seem to be reasonable given the occurrence of large underthrusting earthquakes along the eastern Aleutian trench [Page et al., 1991].

## Discussion

The main driving mechanisms for crustal motion in our models are the geometry and constraints of the PA-NA boundary faults (Aleutian Trench, Fairweather, Queen Charlotte) and the sense of slip of the major inland faults (Denali, Totschunda, Tintina). The differences between models M1 and M2 are not nearly as large as those produced in model M3 where we require that the eastern Aleutian trench act as a pure thrust fault. If we go one step further than model M3 and constrain the eastern Aleutian Trench to be pure thrust at the PA-NA rate, we find left-lateral strike-slip motion on the Contact fault, contrary to geologic observations. This type of scenario would fit the Sumatra type model in which oblique convergence is partitioned into pure thrust motion at the trench and strike-slip motion in the fore-arc [Fitch, 1972; Beck, 1986], although geologic observations in the coastal faults of Alaska find thrust and right-lateral slip.

Model M1 is our preferred model solution. It is the most conservative in its fault constraints and best fits the major active fault systems in Alaska. Models which heavily weigh the VLBI solutions produce solutions with the wrong sense of slip on some of the smaller faults with low slip rates. The VLBI solutions used in this study may contain errors such as site stability (WHIT), unmodeled co-seismic offsets (SOUR), or inter-seismic strain accumulation which are not accounted for in our interpretation of the VLBI solutions [J, Sauber, pers. communication; Sauber et al., 1993]. Some of these differences should go away as more space geodetic data are collected and the solutions improve. A simpler explanation is that our model

does not constrain the faults adequately or that we are missing important faults in our mesh. At this scale of finite element modeling it is the longer (and presumably higher slip-rate) faults which control the deformation pattern; smaller faults such as the **Broxson** Gulch fault act more as passive markers to test our solution. Given the uncertainties in the fault slip rates from both geologic and geodetic methods ( $\pm 3\text{-}4$  mm/yr) and the uncertainties and possible biases in the VLBI solutions ( $\pm 1\text{-}3$  mm/yr) it is encouraging that the major patterns of motion and fault slip rates calculated in our models are within the uncertainties of these observations.

The displacements we calculate for Alaska and NW Canada are a result of the geometric constraints imposed by the shape of the indenting Pacific plate and its oblique convergence with the North America plate along with the constrained motion of the major splays of the **Denali** and **Contact** fault systems. By leaving the rate of slip on the **Denali** fault unconstrained we find that the model predicts a rate of about  $5\text{-}8$  mm/yr for the central **Denali** fault, a higher value than the geodetically derived motion [Ma et al., 1990; Savage and Lisowski, 1991], but lower than the Holocene rates of  $9\text{-}12$  mm/yr [Plafker et al., 1993], and within the uncertainties of both sets of observations. The value calculated in this study is partially controlled by the prescribed rate of  $10 \pm 3$  mm/yr on the nearby **Totschunda** fault and the VLBI rates between sites **GILC** and **SOUR**. Another major constraint is the rate prescribed to the **FairWeather** fault. We use a rate of  $41 \pm 3$  mm/yr on this fault since higher rates produce left-lateral rather than right-lateral motion on the **Chatham Strait** fault. To splay off motion in a right-lateral sense to the **Denali-Chatham Strait** fault the motion on the **Fairweather** fault has to be lower than the overall relative PA-NA motion rate of  $48$  mm/yr. Prescribed rates for the **Fairweather** fault lower than  $41$  mm/yr have the effect of partitioning more right-lateral displacements onto the overriding plate.



The large ( $>10$  mm/yr) crustal motions radiating to the NE away from the Queen Charlotte-Fairweather faults are robust throughout all these models and produce a transverse component at Whitehorse which is very close to the VLBI measured transverse rate (Table 2). Since the only faults in our mesh in that area (Denali-Chatham Strait, Tintina) are constrained to strike-slip motion this motion is accommodated across the Mackenzie Mountains in eastern Yukon and Northwest Territories, an area that has been the locus of several earthquakes greater than magnitude 6 this century and the area of greatest seismicity inboard of the Denali-Chatham Strait fault system [Rogers and Homer, 1991].

The degree to which the Aleutian Trench is constrained has a major effect on the displacements in the North America plate outboard of the Contact fault. When we constrain the plates to converge at the NUVEL-1A [DeMets et al., 1994] rate perpendicular to the trench, the Contact fault becomes entirely left-lateral strike-slip. Model M3 shows that when we relax the constraint on the eastern Aleutian trench we get unacceptably high rates across the Contact fault.

## Conclusions

By incorporating faults and VLBI baselines into the finite element solution for an elastic 2-d spherical shell we calculate displacement rates in Alaska and NW Canada which agree with geologic observations. The patterns of crustal motions we determine produce variations in magnitude and slip directions along fault systems which can explain along-strike differences in the rate observed in the field for fault systems such as the Denali-Chatham Strait. Fundamental to the solution we present is the subduction of the Pacific plate west of Kodiak Island at the NUVEL-1A PA-NA rate and the constraints imposed on the Fairweather and Queen Charlotte faults. The Denali fault is left unconstrained in rate in our preferred model, and we

calculate rates of 5-8 mm/yr for the Denali fault west of the Totschunda fault. Across the Contact fault system we calculate rates around 10 mm/yr, which absorbs much of the displacements generated at the Aleutian trench. The NE directed motion away from the Fairweather-Queen Charlotte faults agrees with VLBI observations at Whitehorse, Yukon, and gets absorbed in our model across the Mackenzie mountains.

The patterns of deformation we calculate in this region are a result of the geometry of the PA-NA boundary and the oblique convergence along the eastern Aleutian trench and the oblique convergence at the Queen Charlotte-Fairweather fault system which transmits compression radially into the North American plate. The complex pattern of motion is partially controlled inland by large scale transcurrent faults which partition motion into strike-slip and compressional fault motion. This partitioning suggests that these large scale transcurrent faults are able to maintain their sense of strike-slip displacements despite their oblique orientation with respect to the relative plate motion direction, and presents a different type of accommodation to the classical Fitch [1972] model: transcurrent motion continues along the major plate bounding faults (Queen Charlotte-Fairweather) with compression absorbed inboard primarily across the Mackenzie Mountains in NW Canada.

The strength of this modeling is that it solves for the motion of the continuum and fault slip rates everywhere in the mesh, producing patterns of motion which can not be produced in simple rigid block models, and calculating fault motions where no field observations exist. Clearly this is but one approach to modeling crustal motions. The validity of any modeling results rests in additional data. Dense geodetic arrays in southern and SE Alaska as well as adjacent areas of Canada would be necessary to refine models of crustal motion and fault slip in this region.

Acknowledgments. We would like to thank John Gipson at GSFC for providing the '93 IERS VLBI solutions and Michael Heflin at JPL for converting them to baseline solutions. We thank Gene Humphreys and Gilles Peltzer for stimulating discussions. Support for P. L., and M.L. was provided by the Jet Propulsion Laboratory, California institute of Technology, under contract to the National Aeronautics and Space Administration.

## References

- Beck, M. E., Model for late Mesozoic-early Tertiary tectonics of coastal California and western Mexico and speculations on the origin of the San Andreas fault, *Tectonics*, 5, 49-64, 1986.
- Biswas, N. N., K. Aki, H. Pulpan, and G. Tytgat, Characteristics of regional stresses in Alaska and neighboring areas, *Geophys. Res. Lett.*, 13, 177-180, 1986.
- Bol, A. J., and S. M. Roeske, Strike-slip faulting and block rotation along the Contact fault system, eastern Prince William sound, Alaska, *Tectonics*, 12, 49-62, 1993.
- Brogan, G. E., L. S. Cluff, K. K. Korringa, and D. B. Slemmons, Active faults of Alaska, *Tectonophys.*, 29, 73-85, 1975.
- Bruns, T.R., and P.R. Carlson, Geology and petroleum potential of the southeast Alaska continental margin, in *Geology and Resource Potential of the Continental Margin of Western North America and Adjacent Ocean Basins-Beaufort Sea to Baja California*, *Earth Sci. Ser.*, vol. 6, edited by D. W. Scholl, A. Grantz, and J. G. Vedder, pp. 269-282, Circum-Pacific Council for Energy and Mineral Resources, Houston, Tex., 1987.
- DeMets, C., R. G. Gordon, D. F. Argus, and S. Stein, Current plate motions, *Geophys. J. Int.*, 101, 425-478, 1990.
- DeMets, C., R. G. Gordon, D. F. Argus, and S. Stein, Effect of recent revisions to the geomagnetic reversal time scale on estimates of current plate motions, *Geophys. Res. Lett.*, 21, 2191-2194, 1994,
- Dixon, T. H., G. Gonzalez, S. M. Lichten, D. M. Tralli, G. E. Ness, and J. P. Dauphin, Preliminary determination of Pacific-North America relative motion in the southern Gulf of California using the Global Positioning System, *Geophys. Res. Lett.*, 18, 861-864,

- 1991,
- Estabrook, C. H., D.B. Stone, and J.N. Davies, Seismotectonics of northern Alaska, *J. Geophys. Res.*, **93**, 12026-12040, 1988.
- Fitch, T. J., Plate convergence, transcurrent faults, and internal deformation adjacent Southeast Asia and the western Pacific, *J. Geophys. Res.*, **77**, 4432-4460, 1972.
- Gabrielse, H., Major dextral transcurrent displacements along the Northern Rocky Mountain Trench and related lineaments in north-central British Columbia, *Geol. Soc. Amer. Bull.*, **96**, 1-14, 1985.
- Gedney, L., and D. Marshall, A rare earthquake sequence in the Kobuk trench, northwestern Alaska, *Bull. Seismol. Soc. Amer.*, **71**, 1587-1592, 1981.
- Gordon, R. G., and S. Stein, Global tectonics and space geodesy, *Science*, **256**, 333-342, 1992.
- Jarrard, R. D., Terrane motion by strike-slip faulting of forearc slivers, *Geology*, **14**, 780-783, 1986.
- Jahr, J. C., and G. Plafker, Holocene Pacific-North America plate interaction in southern Alaska: Implications for the Yakataga seismic gap, *Geology*, **8**, 483-486, 1980.
- Jahr, J. C., R. A. Page, C. D. Stephens, and K. A. Fogleman, Sutton, Alaska, earthquake of 1984: Evidence for activity on the Talkeetna segment of the Castle Mountain fault system, *Bull. Seism. Soc. Amer.*, **76**, 967-983, 1986.
- LeBlanc, G., and R.J. Wetmiller, An evaluation of seismological data available for the Yukon territory and the Mackenzie valley, *Can. J. Earth Sci.*, **11**, 1435-1454, 1974.
- Lisowski, M., J.C. Savage, and R.O. Burford, Strain accumulation across the Fairweather and Totschunda faults, Alaska, *J. Geophys. Res.*, **92**, 11552-11560, 1987.
- Ma, C., J.M. Sauber, L.J. Bell, T.A. Clark, D. Gordon, W.E. Himwich, and J.W. Ryan, Measurement of horizontal motions in Alaska using very long baseline interferometry, *J.*

*Geophys. Res.*, 95, 21991-22011, 1990.

Melosh, H. J., and A. Raefsky, A simple and efficient method for introducing faults into finite element computations, *Bull. Seism. Soc. Amer.*, 71, 1391-1400, 1981.

Melosh, H. J., and D. R. Williams, Mechanics of graben formation in crustal rocks: a finite element analysis, *J. Geophys. Res.*, 94, 13961-13972, 1989.

Page, R. A., N. N. Biswas, J. C. Lahr, and H. Pulpan, Seismicity of continental Alaska, in: D. B. Slommons, E. R. Engdahl, M. D. Zoback, and D. D. Blackwell (Eds.), *Neotectonics of North America*, Geol. Soc. Am., Boulder, Col., 69-76, 1991.

Perez, O. J., and K. H. Jacob, Tectonic model and seismic potential of the eastern Gulf of Alaska and Yakataga seismic gap, *J. Geophys. Res.*, 85, 7132-71 SO, 1980.

Plafker, G., Regional geology and petroleum potential of the northern Gulf of Alaska continental margin, in *Geology and Resource Potential of the Continental Margin of Western North America and Adjacent Ocean Basins-Beaufort Sea to Baja California*, *Earth Sci. Ser.*, vol. 6, edited by D. W. Scholl, A. Grantz, and J. G. Vedder, pp. 229-268, Circum-Pacific Council for Energy and Mineral Resources, Houston, Tex., 1987.

Plafker, G., T. Hudson, and D. H. Richter, Preliminary observations on late Cenezoic displacements along the Totschunda and Denali fault systems, in Blean, K. M., ed., *Geologic studies in Alaska by the U.S. Geological Survey during 1976*, U.S. Geological Survey Circular 751 -B, pp. B67-B69, 1977.

Plafker, G., T. Hudson, T. Bruns, and M. Rubin, Late quaternary offsets along the Fairweather fault and crustal plate interactions in southern Alaska, *Can. J. Earth Sci.*, 15, 805-816, 1978.

Plafker, G., L.M. Gilpin, and J.C. Lahr, Neotectonic map of Alaska, in *Geology of Alaska*, *Geology of North America*, vol. G-1, Geol. Soc. Am., Boulder, Col., plate 12, 1993.

- Rogers, G. C., and R. B. Homer, An overview of western Canadian seismicity, in: D. B. Slemmons, E. R. Engdahl, M. D. Zoback, and D. D. Blackwell (Eds.), *Neotectonics of North America*, Geol. Soc. Am., Boulder, Col., 69-76, 1991,
- Saucier, F., and E. Humphreys, Horizontal crustal deformation in southern California from joint models of geologic and very long baseline. interferometry measurements, in *Contributions of Space Geodesy to Geodynamics: Crustal Dynamics*, Geodynamics 23, D. E. Smith and D. L. Turcotte, eds., pp 139-176, 1993.
- Sauber, J. M., T. A. Clark, L. J. Bell, M. Lisowski, C. Ma, and D. S. Caprette, Geodetic measurements of static displacement associated with the 1987-1988 Gulf of Alaska earthquakes, in *Contributions of Space Geodesy in Geodynamics: Crustal Dynamics*, D. E. Smith and D. L. Turcotte, eds., Geodynamics 23, pp 233-248, 1993.
- Savage, J. C., M. Lisowski, and W.H. Prescott, Strain accumulation across the Denali fault in the Delta River canyon, Alaska, *J. Geophys. Res.*, 86, 1005-1014, 1981.
- Savage, J. C., and M. Lisowski, Strain accumulation along the Denali fault at the Nenana River and Delta River crossings, Alaska, *J. Geophys. Res.*, 96, 14,481-14,492, 1991.
- Smith, D. E., R. Kolenkiewicz, P. J. Dunn, J. W. Robbins, M. H. Torrence, S. M. Klosko, R. G. Williamson, E. C. Pavlis, N. B. Douglas, and S. K. Fricke, Tectonic motion and deformation from Satellite Laser Ranging to I.AGEOS, *J. Geophys. Res.*, 95, 22,013-22,041, 1990.
- Stout, J. H., J. B. Brady, F. Weber, and R. A. Page, Evidence for Quaternary movement on the McKinley strand of the Denali fault in the Delta river area, Alaska, *Geol. Soc. Amer. Bull.*, 84, 939-948, 1973.
- Turcotte, D. L., and G. Schubert, *Geodynamics applications of continuum physics to geological problems*, John Wiley & Sons, New York, 1982.

Zienkiewicz, O. C., and R. L. Taylor, The finite element method, Vol. 1, Basic formulation and linear problems, 4th ed., McGraw Hill, London, 1989.



Figure 1. Oblique Mercator projection about the Pacific-Ninth America rotation pole of the finite element mesh used in this study [DeMets et al., 1990] with the pole located towards the right such that the top and bottom boundaries of the mesh are lines of longitude with respect to that pole and the side boundaries are lines of latitude. Dark lines indicate faults: AT, Aleutian Trench; B, Brooks Range thrust belt; BB, Bruin Bay; BG, Broxson Gulch; C, Contact; CM, Castle Mountain; CS, Chatham Strait; D, Denali; DR, Duke River; EL, Eskimo Lakes; F, Fairweather; INF, Iditarod-Nixon Fork; K, Kaltag; KB, Kigluaik-Bendeleben; KT, Kobuk Trench; MK, Mackenzie mountains faults; P, Pamplona; Q', Queen Charlotte; T, Totschunda; TC, Thompson Creek; TN, Tintina; TZ, Transition Zone. Squares are the locations of the 4 VLBI stations used: GILC, Gilcreek (Fairbanks); NOME, Nome; SOUR, Sourdough; WHIT, Whitchorse.

Figure 2. Model M1. (a) Calculated motions at the center of each element (arrow) and its rate. Also shown are the split nodes with their assigned constraints: *0 dof*, split node constrained in direction and magnitude; *1 dof*, free slip fault node constrained parallel in direction only; *2 dof*, unconstrained fault node. Small squares and their labels give the locations of the VLBI sites. The shading of each element shows the standard deviation in rate for each element after 1000 Monte Carlo runs. (b) Fault rate solution showing the magnitude and sense of motion at fault nodes lying at the middle of element sides.

Figure 3. Model M1 H. The only difference between this model and model M1 is that model M1 H is computed with the VLBI baseline rates weighted at 1000 relative to the surrounding mesh, See Figure 2 caption for explanation of symbols. (a) Motions at the center of each element. (b) Fault motions.

Figure 4. Model M2. The same as model M1 but with the west, central and eastern sections of

the **Denali** fault system are constrained to slip at 11.6, 8.7, and 9 **mm/yr** respectively. See Figure 2 caption for explanation of symbols. (a) Motions at the center of each element. (b) Fault motions.

Figure 5. Model M3. This differs from model M1 in having the eastern Aleutian trench constrained to slip perpendicular to the fault strike and features a truncation of the western extent of the Contact Fault to maintain adequate coupling of the interior and fore-arc regions. See Figure 2 caption for explanation of symbols. (a) Motions at the center of each element. (b) Fault motions.

Table 1. Alaska fault data.

Fault	Rate (mm/a)	$\sigma$	Type	Source
Castle Mountain			RL	<i>a</i>
Contact (E. PWS)			RL	<i>b</i>
Bruin Bay			T	<i>c</i>
<b>Denali central</b>	0			<i>d</i>
<b>Denali central</b>	8.7 †	3 ‡	RL	<i>e</i>
<b>Denali eastern</b>	9	3 ‡	RL	<i>c</i>
<b>Denali western</b>	11.6 †	4 ‡	RL	<i>e</i>
Eskimo Lakes			RL	<i>f</i>
FairWeather	41-51	3	RL	<i>g</i>
FairWeather	58	10	RL	<i>h</i>
<b>Kaltag</b>			RL	<i>i</i>
<b>Kobuk Trench</b>			RL	<i>c</i>
<b>Kobuk Trench</b>			RL	<i>j</i>
Thompson Creek			LL	<i>c</i>
Tintina			RL	<i>i</i>
<b>Totschunda</b>	10	3	RL	<i>g</i>
<b>Totschunda</b>	14.6 †	5 ‡	RL	<i>e</i>

Type: RL, Right-lateral strike-slip; LL, left-lateral; T, thrust. Sources: *a*, Lahr et al., 1986; *b*, Bol and Roeske, 1993; *c*, Plafker et al., 1993; *d*, Savage and Lisowski, 1991; *e*, Plafker et al., 1977; *f*, Leblanc and Wetmiller, 1974; *g*, Lisowski et al., 1987; *h*, Plafker et al., 1978; *i*, Brogan et al., 1975; *j*, Gedney and Marshall, 1981;

† Rate from Plafker et al. [1993] in which they assume 10,000 yr age for fault offsets measured by Plafker et al. [1977].

‡ Since no uncertainties are given for these references an uncertainty was calculated assuming an uncertainty in age to last Pleistocene glaciation of 2000 years and an uncertainty in glacial moraine offset of 10 m. See text for further explanation.

Table 2. VLBI baseline length and transverse rates of change (mm/a) used for this study (J. Gipson, GSFC '93 IERS solution, pers. comm.; baseline velocities computed by M. Heflin, JPL).

Baseline	Observed				Model M1				Model M1H			
	dL/dt	$\sigma$	dT/dt	$\sigma$	dL/dt	$\sigma$	dT/dt	$\sigma$	dL/dt	$\sigma$	dT/dt	$\sigma$
G-N	-2.1	0.7	1.4	<b>0.8</b>	-1.5	0.1	1.5	2.8	-2.0	0.0	2.0	0.5
G-S	1.4	1.1	-7.4	1.3	-4.9	3.4	-3.1	1.7	1.3	0.0	-7.2	0.1
G-W	-9.2	2.5	10.2	2.9	-0.9	0.1	12.6	2.7	-8.1	0.0	<b>11.5</b>	0.5
N-S	-7.1	1.4	-5.1	1.4	-7.4	6.4	2.8	4.7	-7.1	0.0	-4.2	0.7
N-W	-8.9	2.6	13.0	3.0	0.4	0.6	13.4	<b>1.7</b>	-7.4	0.0	14.6	1.6
s - w	-0.9	2.8	17.9	3.1	7.8	<b>5.0</b>	10.8	<b>4.0</b>	-0.5	0.0	18.8	0.2

where VLBI sites are: G, GILC; N, NOME; S, SOUR; W, WHIT

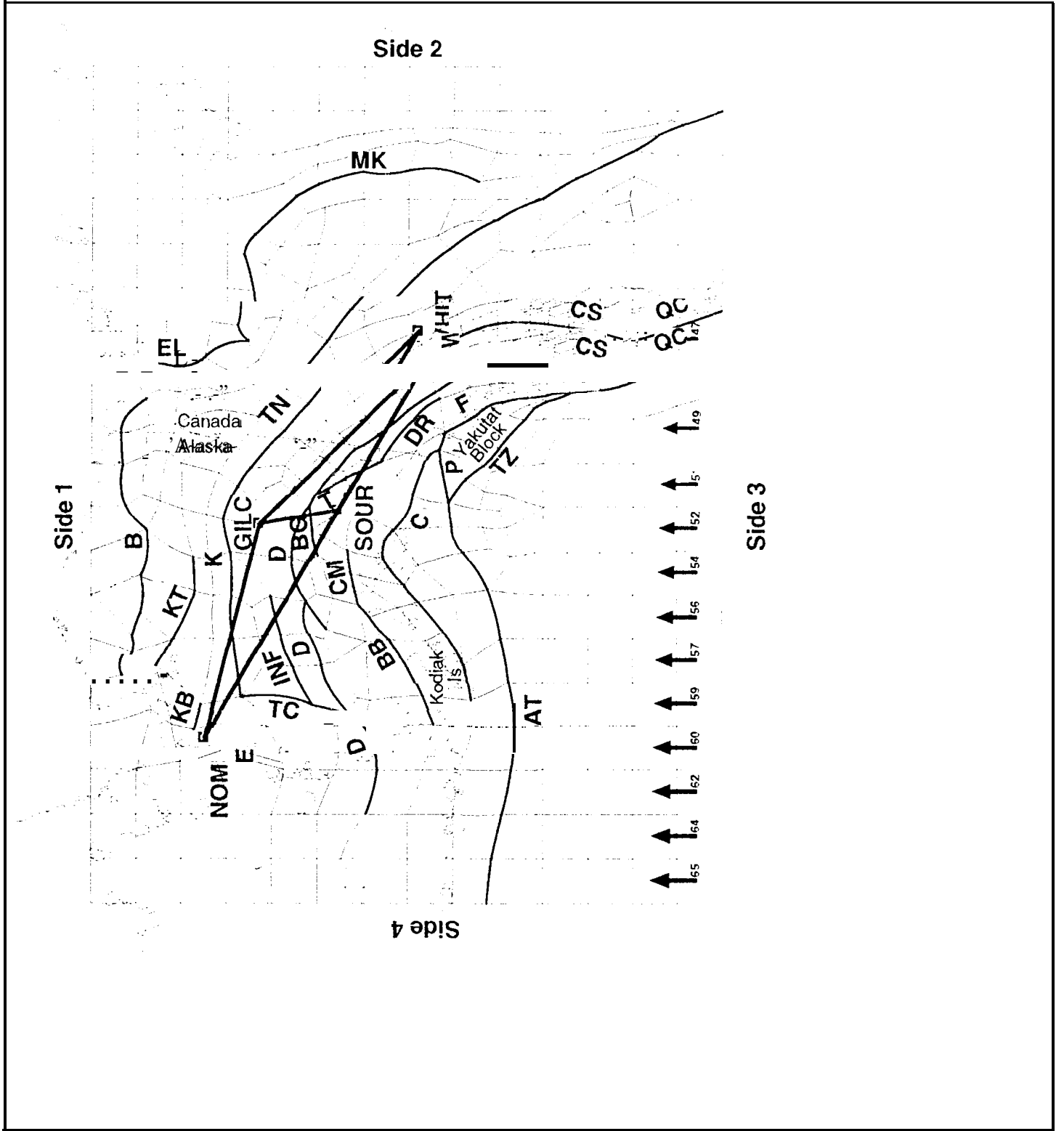
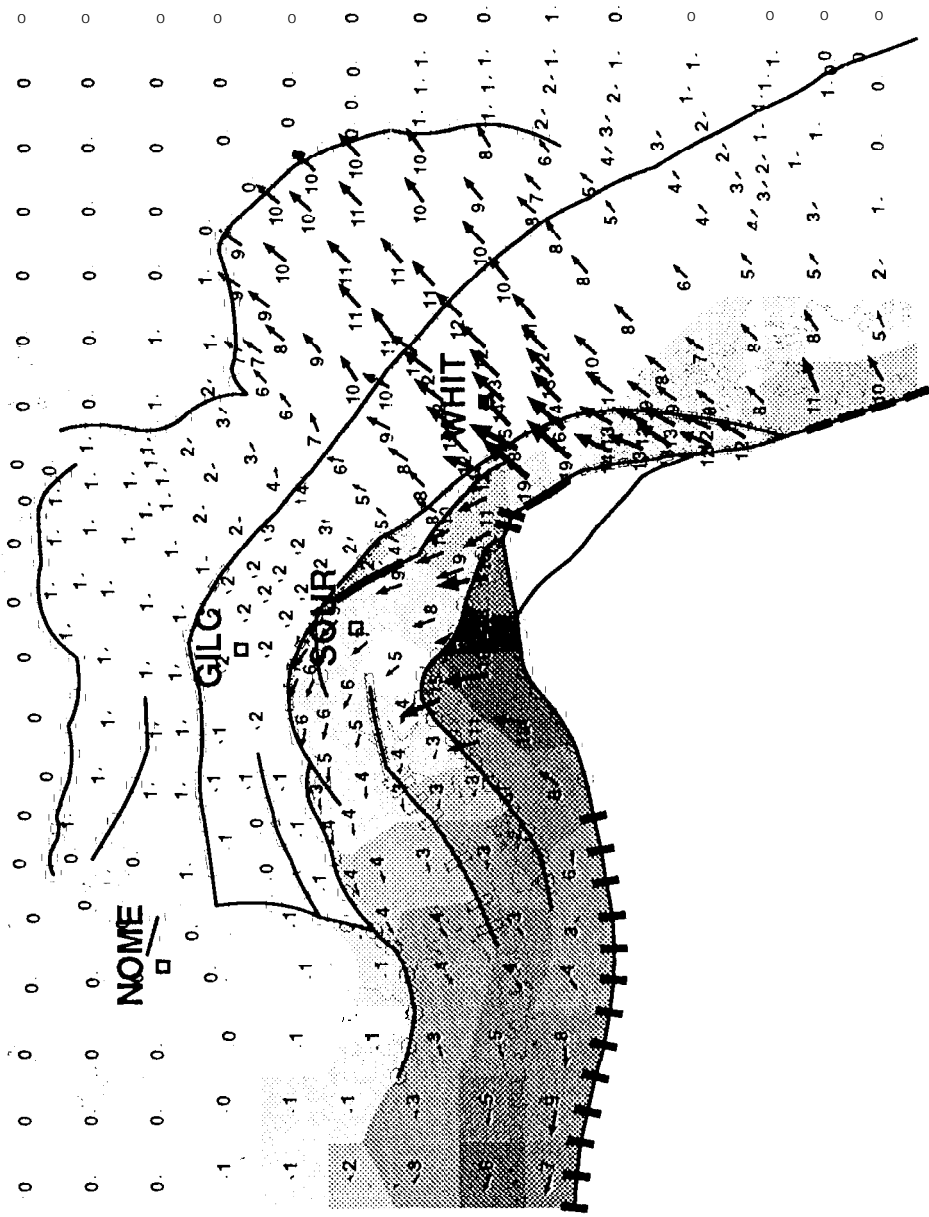
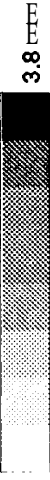


Figure 1



**Model M1**

Plane Stress

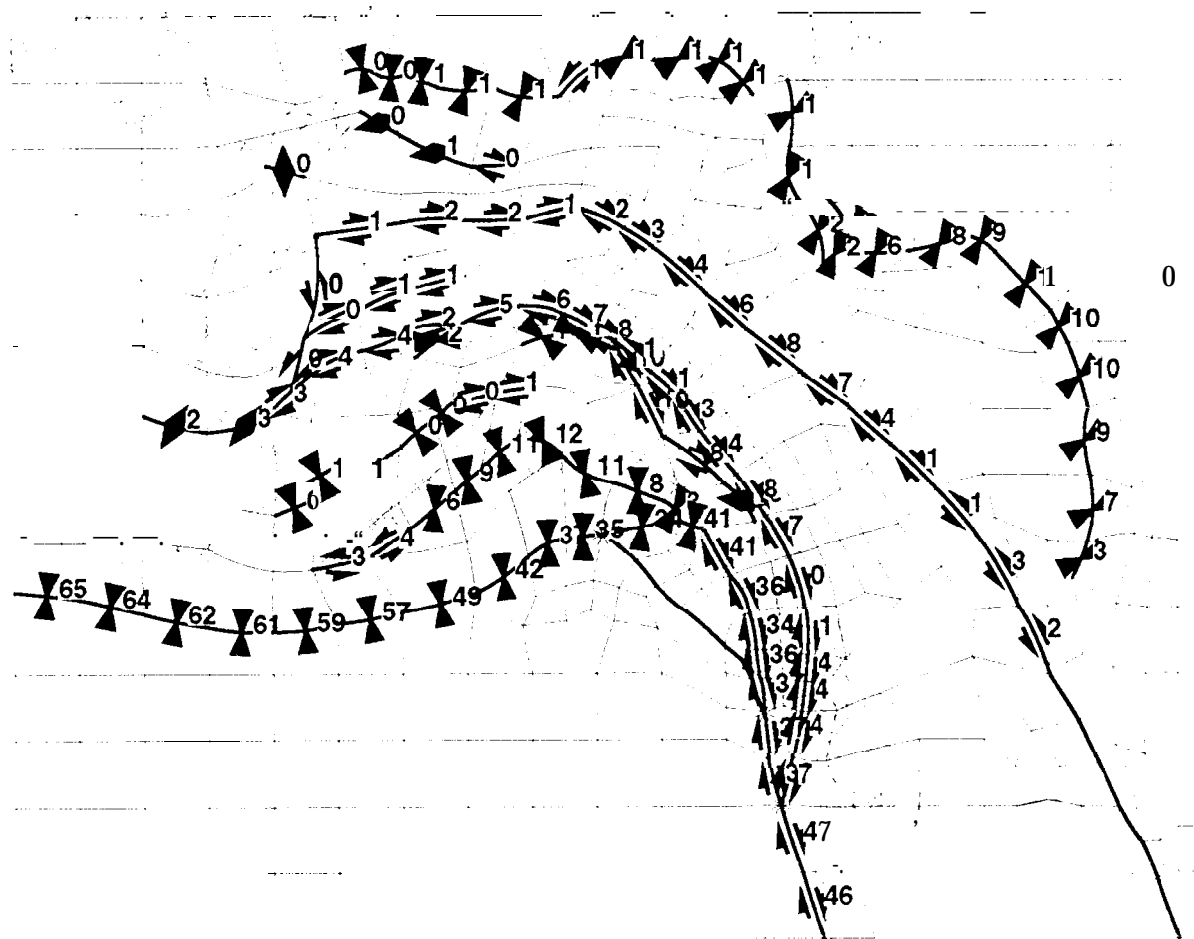


Std. Dev. in magnitude

- Split nodes
- 0 dof
  - - - 1 dof
  - 2 dof
  - △ triple jct

Displacement : 30.00 mm

Figure 2a



**Model M1**

Plane Stress

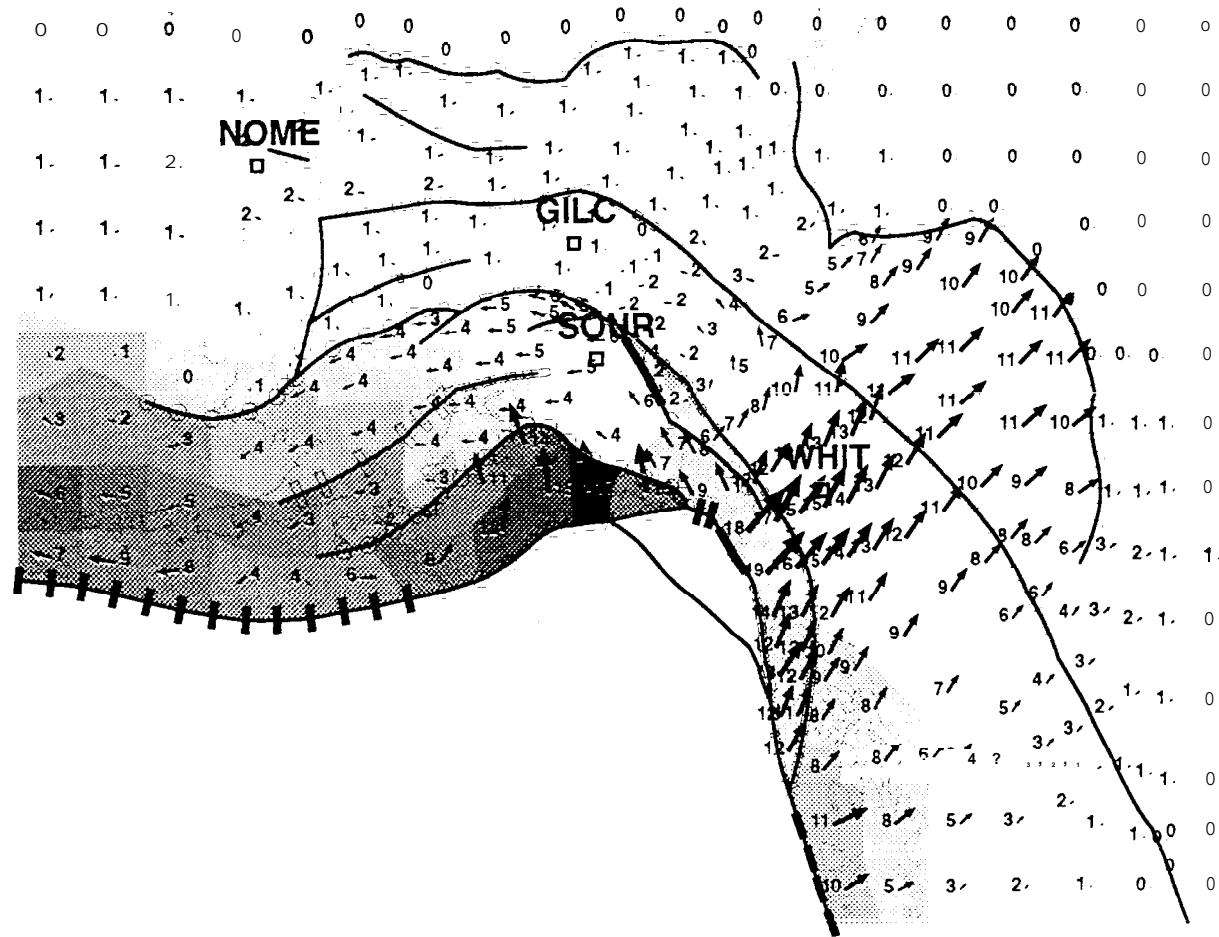
Relative fault motion (mm/yr)

▤ thrust

◆ normal

↔ strike-slip

Figure 2b



**Model MI H**

Plane Stress

Split nodes

- 0 dof
- - - 1 dof
- · · 2 dof
- triple jet



Std. Dev. In magnitude






Displacement: 30.00 mm

Figure 3a





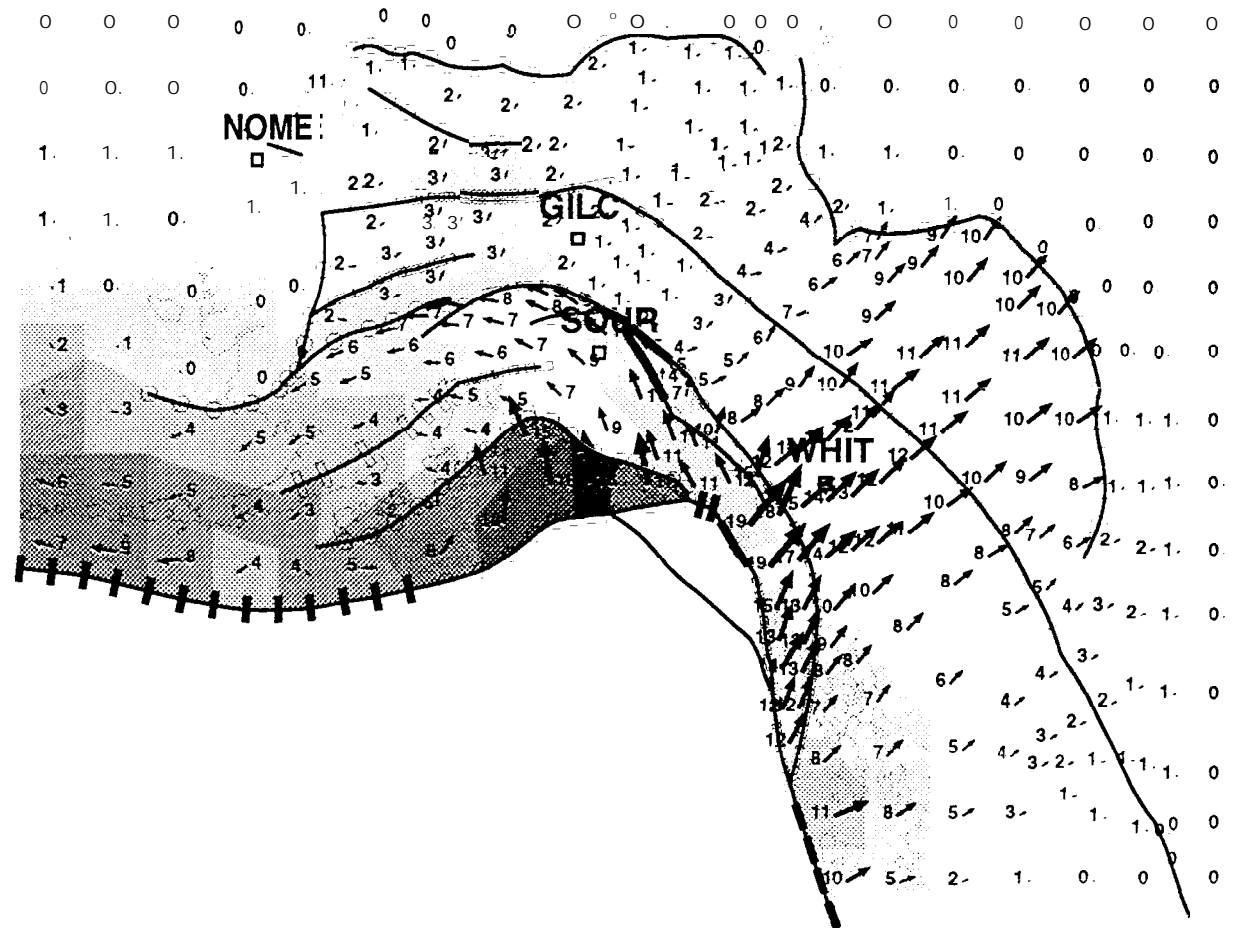
Relative fault motion (mm/yr)

 thrust  
 normal  
 strike-slip

**Model M1H**

Plane Stress

Figure 3:

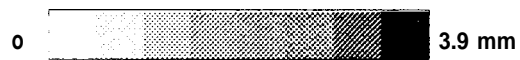


**Model M2**

Plane Stress

Split nodes

- 0 dof
- 1 dof
- 2 dof
- triple jet

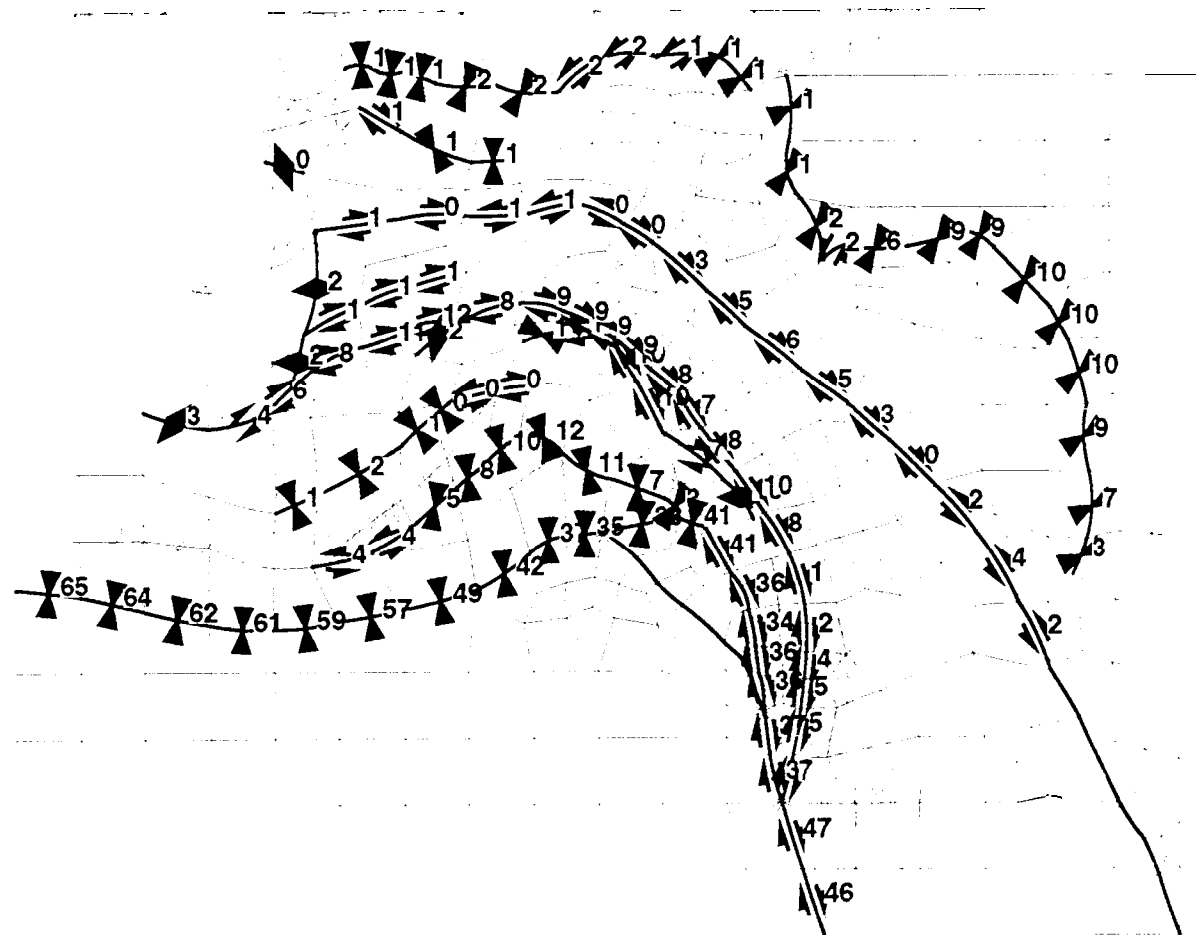


Std. Dev. In magnitude



Displacement :30.00 mm

Figure 4a



**Model M2**

Plane Stress

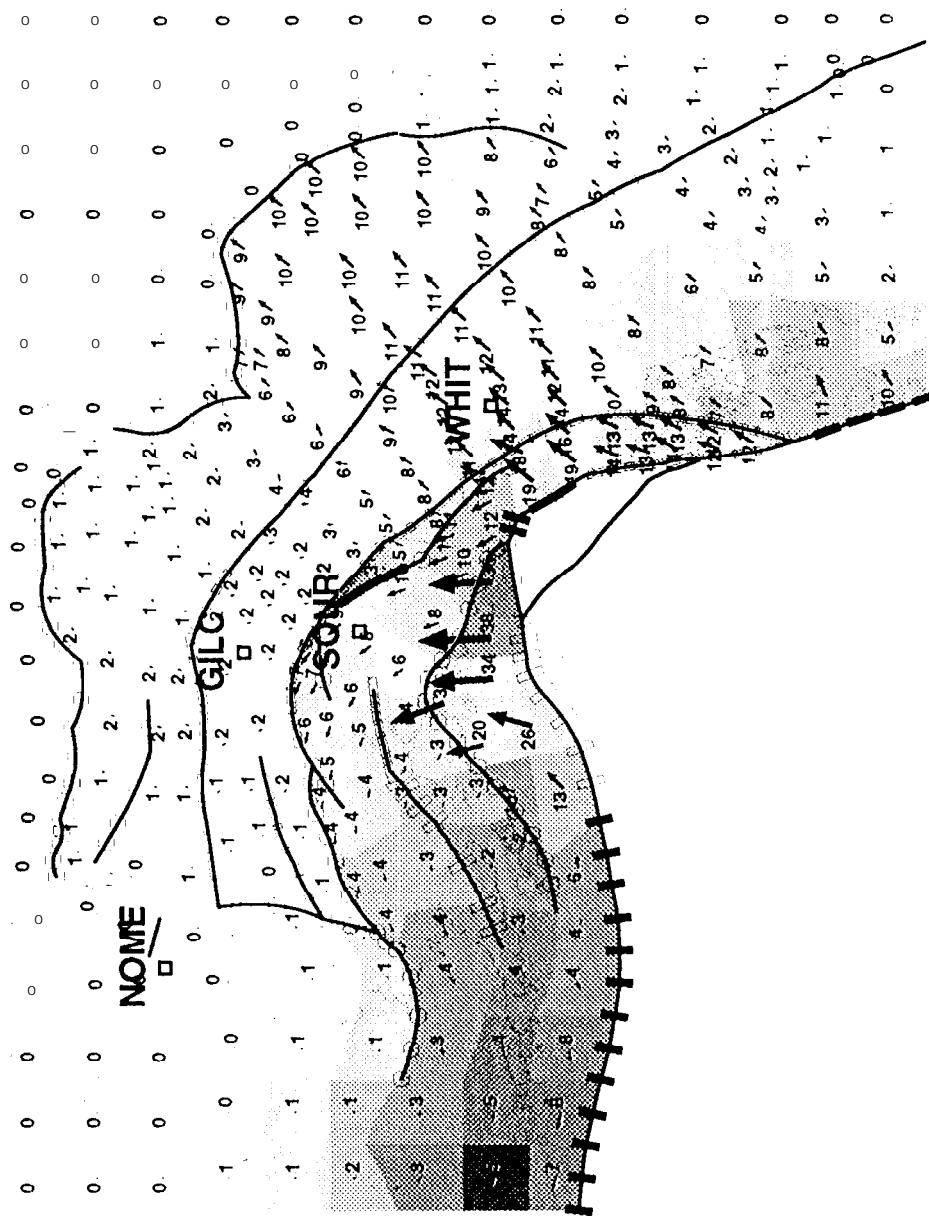
Relative fault motion (mm/yr)

▴▾ thrust

◊◊ normal

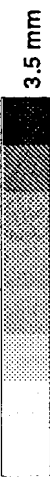
↔ strike-slip

Figure 4b



**Model M3**

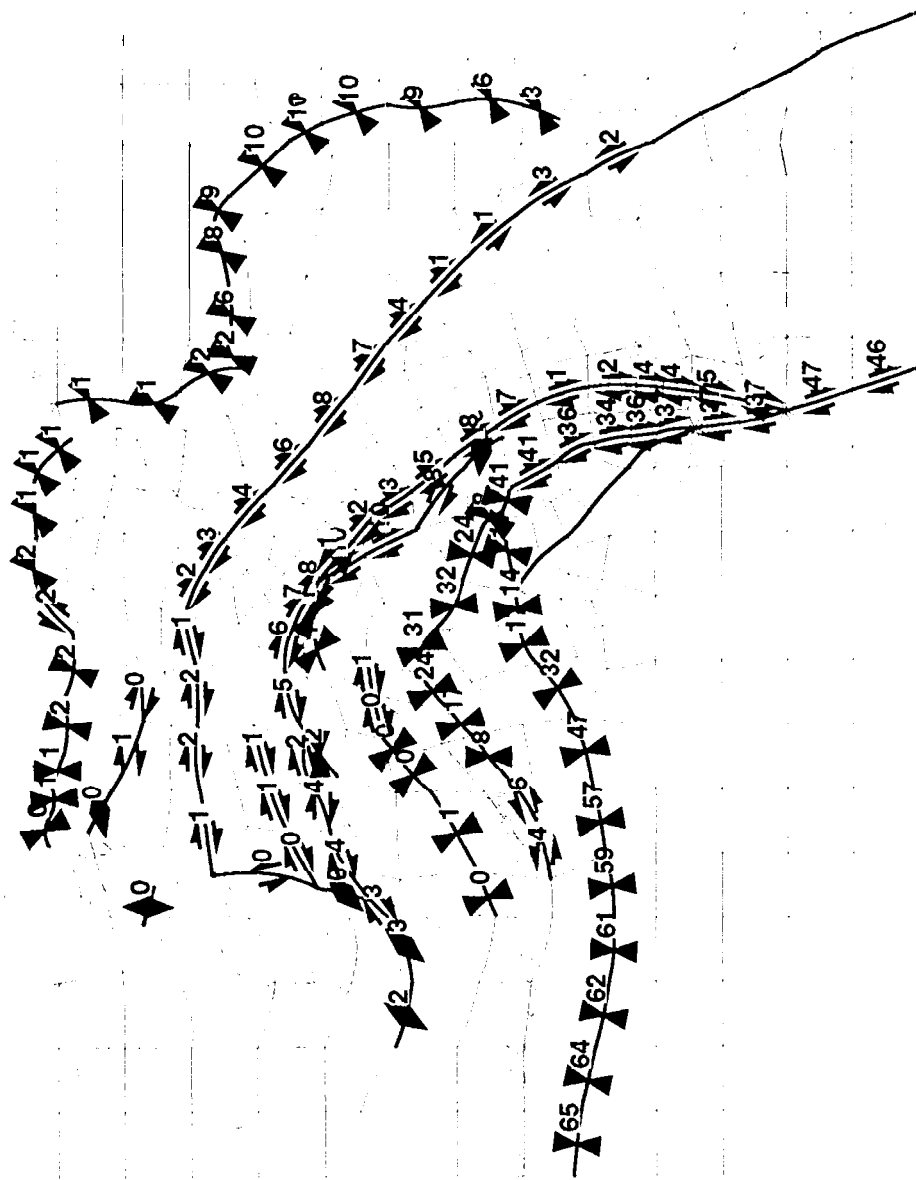
Plane Stress



Std. Dev. in magnitude



Displacement : 40.00 mm



Relative fault motion (mm/yr)

▲ thrust  
 ◆ normal  
 ⇌ strike-slip

**Model M3**  
Plane Stress

Figure 5b